Effective Index Analysis of Bowtie Aperture Plasmonic Waveguides via TM–TE Mode Decomposition

by

UDHAV NAGI

A Project Submitted in Partial Fulfillment of the
Requirements for the Degree of

MASTER OF ENGINEERING

in the Department of Electrical and Computer Engineering

University of Victoria

We acknowledge and respect the Lək̓ʷəŋən (Songhees and Xʷsepsəm/ Esquimalt) Peoples on whose territory the university stands, and the Lək̓ʷəŋən and W̱SÁNEĆ Peoples whose historical relationships with the land continue to this day.

Effective Index Analysis of Bowtie Aperture Plasmonic Waveguides via TM–TE Mode Decomposition

by

UDHAV NAGI

Supervisory Committee

Dr. Reuven Gordon, Supervisor
Department of Electrical and Computer Engineering

Dr. Tao Lu, Departmental Member
Department of Electrical and Computer Engineering

Effective Index Analysis of Bowtie Aperture Plasmonic Waveguides via TM–TE Mode Decomposition

UDHAV NAGI

Department of Electrical and Computer Engineering, University of Victoria, Victoria, BC V8P 5C2, Canada

unagi@uvic.ca

***Abstract* – A Modified Effective Index Method (MEIM) is presented for determining the propagation constant of nanoscale bowtie aperture waveguides operating across the $500 - 1000\ nm$ spectral range. The approach uses staircase discretization to approximate the tapered bowtie geometry and employs a geometry-driven formulation to maintain numerical stability for sub-$30\ nm$ features. The transverse-magnetic (TM) response is computed using the hyperbolic-tangent dispersion relation for a three-layer metal–insulator–metal (MIM) stack, while the transverse-electric (TE) contribution is incorporated using a multi-slab transfer-matrix method (TMM) that enforces field continuity across discretized slabs. By combining these formulations, the model reproduces the expected plasmonic behaviour, including a monotonic decrease in effective index with increasing wavelength and stronger confinement for smaller bowtie gaps. Using wavelength-dependent silver permittivity data, the MEIM results agree well with the rectangular-slab reference problem, confirming the correctness of both the TM and TE formulations. The framework remains computationally efficient, physically interpretable, and easily extendable to other subwavelength apertures, offering a useful preliminary design tool for plasmonic waveguides and sensing structures.**

Keywords – Modified Effective Index Method (MEIM), propagation constant, bowtie aperture waveguide, geometry-driven, sub-30nm features, metal-insulator-metal, transfer-matrix method.

1. INTRODUCTION

1.1. Refractive and Effective Indices in Guided-Wave Optics

The refractive index η of a material describes how much the speed of an electromagnetic (EM) wave slows down compared to its speed in vacuum [1]. It is an intrinsic property determined by the material's electronic structure. In guided-wave optics, light propagation is usually characterized by an effective refractive index, which represents the overall phase delay

experienced by a mode within the guiding structure. This effective refractive index is not solely a property of the material itself, but a combination of the optical material along with its specific geometry and boundary conditions.

Building on this concept, the Effective Index Method (EIM) is a modelling approach that describes guided propagation in waveguides. EIMs process is to convert a two-dimensional waveguide into its one-dimensional equivalents, with an effective index profile derivable from the original structure's refractive index profile [2] illustrated in Fig. 1. EIM is an approximation technique, since exact solutions to Maxwell's equations that satisfy the boundary conditions for real metals are analytically impossible to achieve [3],[4]. This method is mainly used for its ease of implementation and the short computational time required to model a structure [5].

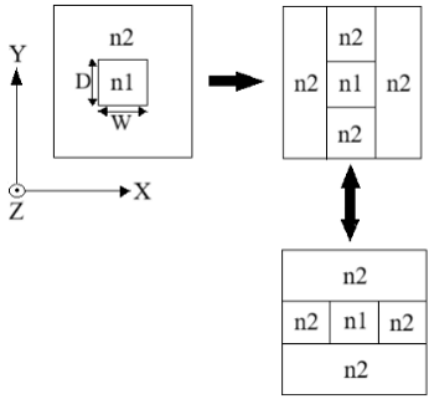

Fig. 1. Configuration of a rectangular waveguide and schematic descriptions of Effective Index Method

1.2. Purpose and Applications of the Effective Index Method

The Effective Index Method is used to calculate the propagation constant β and the effective refractive index η_{eff} for different buried waveguide geometries, accounting for realistic refractive index contrasts and various layer configurations. EIM is widely used in integrated optics and fiber waveguide analysis, especially for asymmetric, multilayered, or buried waveguides (e.g., rectangular, ridge, or trench types), where full-vector finite-element or finite-difference solutions are computationally intensive.

In the context of application domains, accurately determining the effective and group refractive indices η_{eff} and η_g of optical waveguides as a function of wavelength is critical for the design of photonic integrated circuits (PICs). Since a large number of simulation iterations are performed

during PIC design, simulation methods that rely on approximations such as EIM are required. PICs find applications in the fields of microwaves, telecommunications, and sensing [6],[7].

EIM is an essential modelling tool for passive waveguide-based devices. In directional couplers, it enables estimation of coupling coefficients between adjacent waveguides [8]. In optical splitters, it provides the means to analyze mode propagation and field distributions. EIM can also be used in active photonic devices. For instance, in the case of high-power injection lasers, EIM can predict optical confinement factors without solving the full vector Maxwell equations in all dimensions [9].

1.3. Project Overview

This project contains an analysis using a modified Effective Index Method integrated with the staircase approximation to determine the propagation constant of a nanoscale bowtie-shaped waveguide [10] as shown in Fig. 2. By extending the EIM to a non-separable, hybrid plasmonic configuration, the study bridges the gap between purely numerical techniques and analytical modelling.

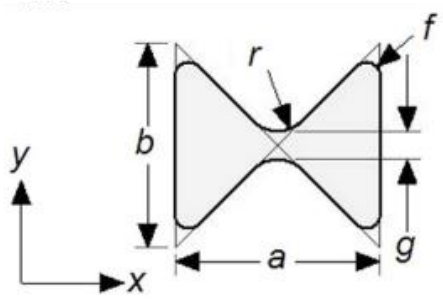

Fig. 2. Bowtie Aperture Geometry [10]

A bowtie aperture consists of two opposing triangular cuts in a metal film that form a narrow central gap. These apertures are becoming increasingly important in nanophotonics and plasmonics due to their ability to focus electrometric fields below the diffraction limit. This capability has generated substantial theoretical and experimental interest [11],[12]. Nanoscale bowtie apertures have found applications in nanoantennas [13] and nanolithography [14] because they can focus light well below the diffraction limit with extremely high transmission efficiencies. They are generally used where field enhancement and high optical resolution are of utmost importance. Understanding their modal behaviour through an analytical framework such as EIM

can significantly reduce design complexity and accelerate the optimization of nanoscale optical components**.**

The findings from this study hold theoretical and practical value. On the theoretical side, the work extends EIM to address complex plasmonic geometries. Practically, the approach provides a faster way for researchers to approximate modal behaviour without relying on intensive numerical simulations. In doing so, it provides a valuable framework for designing and refining nanophotonic and plasmonic components, enabling faster modelling and optimization of next-generation optical devices.

2. LITERATURE REVIEW

2.1. Theoretical Background

The propagation of light within optical and plasmonic waveguides is fundamentally governed by Maxwell's equations, which describe the relationship between electric and magnetic fields in space and time. For a linear and isotropic dielectric waveguide characterized by a spatial permittivity distribution ϵ, Maxwell's equations are shown in Eqs. (1) to (4):

$$\nabla \times \boldsymbol{E} = -\mu_0 \frac{\partial \boldsymbol{H}}{\partial t} \tag{1}$$

$$\nabla \times \boldsymbol{H} = \epsilon \frac{\partial \boldsymbol{E}}{\partial t} \tag{2}$$

$$\nabla \cdot (\epsilon \mathbf{E}) = 0 \tag{3}$$

$$\nabla \cdot \boldsymbol{H} = 0 \tag{4}$$

where $\boldsymbol{E}$ and $\boldsymbol{H}$ represent the electric and magnetic field vectors, and μ_0 denotes the absolute permeability of vacuum.

Applying the vector identity $\nabla \times (\nabla \times \boldsymbol{A}) = \nabla(\nabla \cdot \boldsymbol{A}) - \nabla^2 \boldsymbol{A}$ to the Maxwell equations stated above results in:

$$\nabla^2 \boldsymbol{E} + k^2 \boldsymbol{E} = -\nabla\left(\frac{\nabla \epsilon}{\epsilon} \cdot \boldsymbol{E}\right) \tag{5}$$

Where $k = 2\pi/\lambda$ is the wavenumber, the homogeneous wave equation for each region can be expressed as:

$$\frac{\partial^2 E_z}{\partial x^2} + \frac{\partial^2 E_z}{\partial y^2} + (k^2 - \beta^2) E_z = 0 \tag{6}$$

Here, β is the propagation constant of the mode. The EIM, introduced by Marcatili [15] and later refined by Snyder and Love [16] reduces the 2-D Helmholtz equation (Eq. 6) to a series 1-D problems. Assuming weak coupling between orthogonal field components, the modal field can be approximated as:

$$E(x, y) \approx X(x) Y(y) \tag{7}$$

With this approach, the vertical and lateral confinements can be handled separately. When the 1-D problems are solved using the usual slab-waveguide boundary conditions, they give rise to a set of discrete guided modes, each with its own effective refractive index.

$$\eta_{eff(x,y)} = \frac{\beta_{x,y}}{k_0} \tag{8}$$

The $\eta_{eff(x,y)}$ represents the average optical confinement of the field in the vertical or horizontal direction and effectively "compresses" the information of that dimension into a single refractive-index value.

2.2. Polarization Considerations

In optical waveguides, the field orientation relative to the propagation direction defines the polarization. For transverse electric (TE) modes, the electric field has no component in the direction of propagation ($E_z = 0$), while a magnetic field does have a component in that direction. It is also called "E-less" mode. Similarly, for transverse magnetic (TM) modes, there is no component of the magnetic field in the direction of propagation ($H_z = 0$), while the electric field does; hence, it is called an "E-component" mode [17].

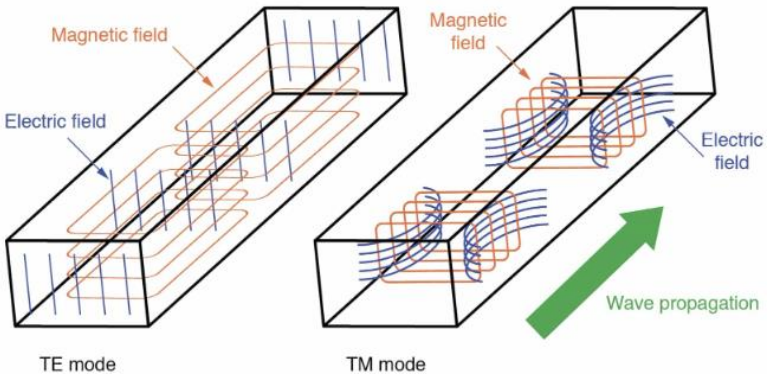

Fig. 3. Representation of Electric and Magnetic Fields in TE and TM Modes [28]

In a planar slab, TE and TM modes are separable and orthogonal in nature. In contrast, real 2-D structures such as rib or double nanohole waveguides have asymmetric refractive-index profiles; hence, both components are non-zero. The resulting modes are thus quasi-TE or quasi-TM [18], rather than purely TE or TM.

Fig. 4 illustrates two sequences in which EIM can be executed. In the TM–TE method, we first consider a simple slab structure with refractive index variation in the Y-direction (vertically) to obtain an effective refractive index $\eta_{eff,y}$. Then, refractive index variation in the X-direction (horizontally) is used to solve for the total effective refractive index η_{eff} and the total propagation constant β_T. In the TE–TM method, the sequence is reversed [19]. The results obtained with these two methods differ due to different boundary conditions at material interfaces.

Consequently, the EIM should be interpreted as a semi-vectorial approximation, yielding physically meaningful but polarization-averaged effective indices. In practice, the TE–TM and TM–TE results are usually treated as upper and lower bounds for the true modal effective index obtained from full-vector numerical solvers such as FEM or FDTD.

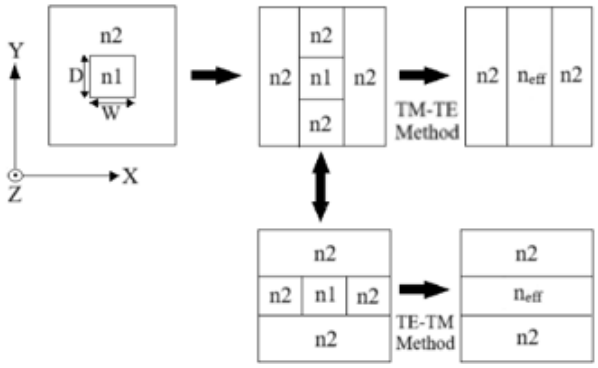

Fig. 4. Configuration of a rectangular waveguide and schematic descriptions of Effective Index Method using TM-TE and TE-TM methods.

2.3. Limitations in the Conventional Effective Index Method

Even though the Effective Index Method is widely used in the modelling of integrated optics, it has several limitations that can restrict its range of applications and accuracy. The assumption of separable fields $E(x,y) \approx X(x)Y(y)$ holds only when the interaction between the two dimensions is weak and the index gradients are small [15]; otherwise, it fails, as noted for asymmetric, or metal–dielectric structures. Yielding errors in the propagation constant β and effective refractive index η_{eff} [20].

Another limitation is EIM's inability to treat regions whose thickness lies below the cutoff for guided propagation. If the waveguide is thinner than this cutoff, the mode physically cannot exist. However, the method continues to assign an "effective" index as if confinement were

present. This leads to non-physical results near the cutoff. EIM tends to predict stronger guidance and higher η_{eff} than actually present, leading to a deviation of $3-5\%$. Such inaccuracies are observed in rib and trench geometries [21], [22], which distort predictions of coupling length and dispersion. The discrepancy grows with increasing asymmetry.

In addition, EIM is sensitive to the refractive-index contrast of the environment [23]. It works well when the structure is surrounded by air, but its accuracy drops if the fiber or waveguide is placed in a liquid with a refractive index close to the cladding. When the difference between the core and cladding indices is small, the EM field spreads out more, becoming less confined. As a result, the effective index contrast diminishes, and EIM's slab-based approximation no longer holds.

2.4. Historical Evolution and Emerging Need to Modify the Effective Index Method

Since the inception of the Effective Index Method, it has advanced to the point where it can be used in photonic devices. Marcatili focussed on low-index rectangular guides [15], while Snyder and Love generalized it to asymmetric multilayer systems [16], and Chiang improved the numerical accuracy for rectangular geometries [20]. Ramaswamy and Srivastava [21] and Marcuse [22] adapted the method for rib and buried structures, while Kumar and Srivastava [24] enhanced convergence through an iterative refinement.

EIM's principles were extended into plasmonic domains by Oulton et al. [25] and Berini [26], incorporating complex permittivities and metal–dielectric coupling into hybrid analytical models. However, these approaches were mostly restricted to planar slot geometries and did not provide a generalized framework for non-separable structures such as triangular or bowtie apertures, where strong inter-wedge coupling plays a significant role.

The bowtie aperture waveguide represents an extreme case: two tapered wedges that form a nanoscale gap, supporting hybrid plasmonic modes with significant longitudinal fields. Conventional EIM cannot capture these effects, nor can it handle regions below the cutoff thickness where no guided modes exist. These shortcomings, combined with the need for rapid, analytical modelling in nanophotonic design, motivate the development of a Modified Effective Index Method (MEIM).

Over time, the Effective Index Method (EIM) has developed from a basic weak-guidance model into a more advanced, near-vector approach. Building on this progress, this study applies EIM to nanoscale bowtie-aperture waveguides, aiming to balance analytical simplicity with increased accuracy, approaching that of full-vector numerical methods. The following section explains the methodology, including the mathematical steps behind the modified EIM and how the staircase approximation method is used.

3. METHODOLOGY

3.1. Approach Overview

To apply the Modified Effective Index Method (MEIM), the bowtie waveguide is discretized into multiple layers using a staircase approximation. Each layer is treated as an individual slab waveguide, and the resulting effective indices are then combined to estimate the overall propagation constant and effective refractive index η_{eff}. This strategy preserves the analytical efficiency of EIM while incorporating the effects of complex geometry, plasmonic dispersion, and sub-cutoff behaviour characteristic of nanoscale structures. The simulations are implemented in MATLAB, which provides robust matrix-handling capabilities and integrates well with optical modelling workflows. In this way, the method retains the simplicity of traditional EIM while extending its applicability to plasmonic systems for which full-vector numerical solvers are computationally demanding.

3.2. Geometry and Discretization

In this project, the bowtie aperture consists of two silver (Ag) wedges facing each other, separated by an air gap of width g in between. The wavelength-dependent permittivity of silver, ϵ_m, is taken from Johnson and Christy's data [27], and the inner region is treated as air with $\epsilon_{\text{air}} \approx 1.006 \approx 1$. The simulation focuses on wavelengths between $500\ nm$ and $1000\ nm$, covering the visible range and extending into the near-infrared (NIR). Across this band, silver shows strong plasmonic behaviour because its real permittivity stays large and negative while the imaginary part remains comparatively small. At the lower end of the range (around $500\ nm - 600\ nm$), losses start to increase due to interband transitions in the metal. On the higher-wavelength side (around $900\ nm - 1000\ nm$), the plasmonic confinement gradually weakens as silver begins to behave more like a near-perfect conductor, reducing the field enhancement inside the aperture [4].

In this study, the bowtie dimensions were chosen to stay consistent with what has been used in earlier work [10]. The aperture width and height were kept equal ($a = b$) and varied together at $150\ nm$, $200\ nm$, and $250\ nm$. Using the same value for both dimensions keeps the geometry simple and lets the structure scale in a clean, uniform way. It also makes it easier to compare the results with the existing literature. By adjusting only $a = b$, the analysis avoids introducing extra assumptions and focuses directly on how the overall aperture size influences the effective index.

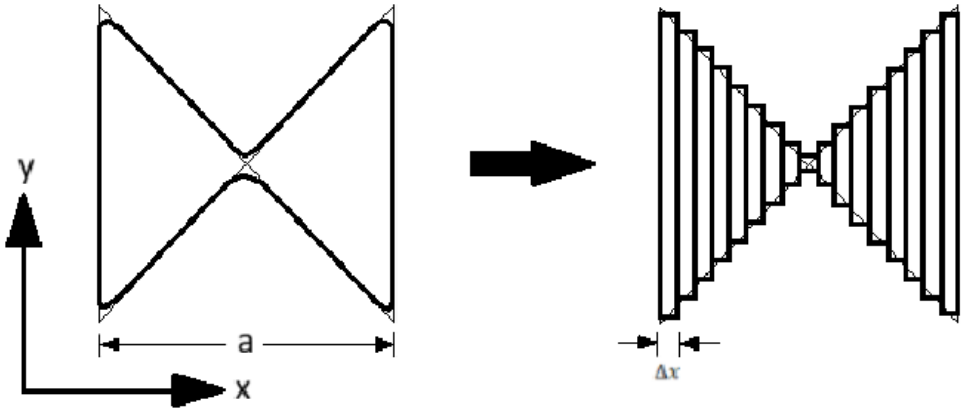

Fig. 5. Pictorial Description of TM-Mode Discretization for the Bowtie aperture, with bowtie width a being discretized into many rectangular slabs of width Δx

3.2.1. Bowtie Gap-Height Function

To incorporate the bowtie shape into MEIM, the two-dimensional aperture is reduced to a one-dimensional height function $w(x)$, which describes the local gap at each lateral coordinate x. The minimum gap is computed following the analytic geometric expression from Ding et al [10].

$$g = 2r\left(\frac{1}{a}\sqrt{a^2 + b^2} - 1\right) \tag{9}$$

Where r is the apex curvature radius, considered to be 30nm.

The local gap height increases linearly away from the center:

$$w(x) = g + (b - g)\frac{2|x|}{a}, \quad |x| \leq \frac{a}{2} \tag{10}$$

This provides a clean and manageable way to approximate the bowtie taper. In practice, the field is most tightly confined near the narrow center of the aperture and slowly spreads out as the structure widens toward the edges. Using a staircase approximation, $w(x)$ is sampled into N uniform lateral slices, as shown in Eq. 11.

$$\{w_1, w_2, \ldots, w_N\}, \quad x_i = -\frac{a}{2} + \left(i - \frac{1}{2}\right)\frac{a}{N} \tag{11}$$

Each discretized layer is handled separately using MEIM. For each slice, TM analysis is applied in the vertical direction and TE analysis in the horizontal direction to determine the local propagation constant and effective index. These slice-wise values are then combined to obtain the overall η_{eff} of the bowtie. This layered approach lets the model track how the confinement and field distribution change in each slab while still maintaining the curved geometry's physical accuracy.

3.3. TM Mathematical Formulation

In metal–air–metal structures, the dominant fields are TM in nature, with strong normal electric-field components at metal interfaces. Starting with the TM step ensures that the plasmonic boundary conditions and field confinement are accurately captured before refining the lateral (TE-like) behaviour. The TM-mode dispersion is:

$$\tanh\left(\sqrt{\beta_{TM}^2 - k_0^2\epsilon_{air}}\frac{w_i}{2}\right) = -\frac{\epsilon_{air}}{\epsilon_m(\lambda)}\frac{\sqrt{\beta_{TM}^2 - k_0^2\epsilon_m}}{\sqrt{\beta_{TM}^2 - k_0^2\epsilon_{air}}} \tag{12}$$

Here, $\beta_{TM} = \eta_{eff,TM}k_0$ is the propagation constant of the TM Mode and $k_0 = 2\pi/\lambda$. This equation is solved iteratively for each slice until the residual approaches zero. The resulting $\eta_{eff,TM}(x_i, \lambda)$ defines the effective permittivity of each slice which incorporates the correct plasmonic dispersion for each local gap size:

$$\epsilon_d(x_i, \lambda) = \eta_{eff,TM}(x_i, \lambda)^2 \tag{13}$$

The TM mode formulation is appropriate for this project because the bowtie aperture can be treated locally as a three-layer structure. Since Eq. 12 [4] is derived for a 3-layer geometry, it can be directly applied to each vertical slice in the staircase approximation without additional modification.

3.4. TE Mathematical Formulation through Transfer Matrix Method

For the TE polarization, the lateral direction x is treated as a stack of thin dielectric slabs, each defined by an effective permittivity $\epsilon_d(x_i, \lambda)$ obtained from the TM vertical solution. These slabs form a one-dimensional inhomogeneous waveguide bounded by metal on both sides:

$$metal\left|\epsilon_{d,1}, \epsilon_{d,2}, \ldots, \epsilon_{d,N}\right|metal$$

3.4.1. Transfer Matrix Construction

For a slice with permittivity $\epsilon_d(i)$ and lateral wavenumber $k_{x,i} = \sqrt{\epsilon_d(i)k_0^2 - \beta_{TM}^2}$, the propagation matrix is:

$$P_i = \begin{bmatrix} \exp(ik_{x,i}\Delta x), & 0 \\ 0 & \exp(-ik_{x,i}\Delta x) \end{bmatrix} \tag{14}$$

At each interface between slices i and $i+1$, the TE Interface matrix is:

$$L_{i\to i+1} = \frac{1}{2}\begin{bmatrix} 1+\kappa\eta & 1-\kappa\eta \\ 1-\kappa\eta & 1+\kappa\eta \end{bmatrix} \tag{15}$$

Where $\kappa = k_{x,i}/k_{x,i+1}$ and $\eta = \epsilon_d(i+1)/\epsilon_d(i)$.

The full lateral transfer matrix is:

$$M = L_{0\to 1}P_1L_{1\to 2}P_2 \dots P_N L_{N\to N+1} \tag{16}$$

Where region 0 and $N+1$ are metal (Silver)

3.4.2. Mode Condition via Residual Minimization

In TE Mode theory, the transfer matrix must be normalized, and we apply a physical radiation condition that allows only decaying waves in the cladding. In the left metal, a physically allowed TE Mode must have a forward-decaying wave present and a backward-decaying wave suppressed. This corresponds to a left-hand field vector:

$$v_{left} = \begin{bmatrix} 1 \\ 0 \end{bmatrix} \tag{17}$$

Relating left and right boundary fields:

$$v_{left} = Mv_{right} \tag{18}$$

Solving gives the condition for a guided mode in Transfer Matrix Method:

$$M_{21} = 0 \tag{19}$$

Hence, the dispersion relation for TE Modes in multilayer stacks occurs when the (2,1)-element of the global transfer matrix vanishes. This gives us the residual:

$$R(\beta_{TM}) = |M_{21}(\beta_{TM})| \rightarrow 0 \tag{20}$$

The effective index is the value of $\beta_T = \eta_{eff,TE} k_0$ where this quantity is minimized. If the minimum residual is below a tolerance $\approx 10^{-2}$, the TE mode is considered supported; otherwise, it is cut off.

Because higher wavelengths produce weaker confinement, a cutoff occurs when the TE residual cannot reach the tolerance threshold. In this approach, while cutoff wavelengths are estimated through transfer matrix method, a backup formula was used to ensure the mode does not propagate post cutoff, this was done using the formula in Eq. 21.

$$\lambda_{cut} = \frac{\pi L \sqrt{\epsilon_d}}{\tan^{-1}\left(\sqrt{-\frac{\epsilon_m}{\epsilon_d}}\right)} \tag{21}$$

The cut-off wavelength was evaluated using the permittivity of the central slice.

3.5. MATLAB Implementation and flow diagram

The complete computational sequence of the Modified Effective Index Method is illustrated in Fig. 6. It outlines the stepwise approach, from defining geometric and material parameters, to solving the TM and TE dispersion relations, and finally averaging the results to obtain the global effective index. This schematic serves as a concise visual summary of the iterative process used to model and analyze the bowtie aperture waveguide.

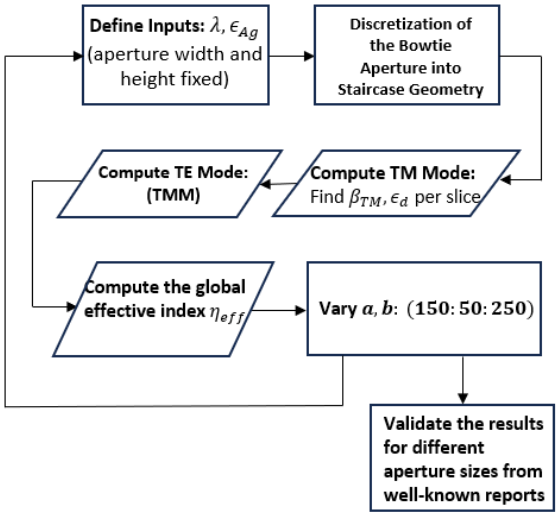

Fig. 6. Block Flow Diagram of the Computational Procedure for the Modified Effective Index Method

4. RESULTS AND FINDINGS

4.1. Overview of Simulation Setup

The bowtie aperture was discretized laterally into a finite number of slices. Each slice represents a vertical metal–insulator–metal (MIM) sub-waveguide for the TM mode, and the resulting effective permittivities were then used as inputs for the TE transfer-matrix solver. Three different bowtie sizes were simulated. Aperture width a and aperture height b were kept equal. The aperture size was increased in increments of $50\ nm$ in the range of $150\ nm$ to $250\ nm$.

The simulations were performed over the wavelength range $500 - 1000\ nm$ using the interpolated Johnson-Christy permittivity dataset [27] for silver. Silver remains plasmonic (negative real permittivity) across the entire operating band, enabling tightly confined TM-like fields in the aperture and providing meaningful data for the hybrid MEIM approach.

A staircase approximation approach was utilized to represent the tapered bowtie profile, with the geometry divided into 12 lateral slices. This number was selected as an optimal compromise between accurately capturing the shape of the bowtie and ensuring numerical stability while performing the simulations. Additional justification for this choice is provided in the Discussion section.

4.2. TM Mode Effective Index and Validation

The TM mode was solved independently in each lateral slice by treating the aperture locally as a three-layer Metal-Insulator-Metal (MIM) configuration, using a well-established tanh dispersion relation as mentioned in Eq. 12. This is valid because every vertical cross-section of the bowtie geometry is effectively a symmetric and rectangular MIM slot with its own local thickness $w(x)$.

For all three geometries, the TM effective permittivity $\epsilon_d(\lambda, x) = \eta_{eff,TM}^2$ exhibited the expected plasmonic trends, as also shown in Fig. 7.

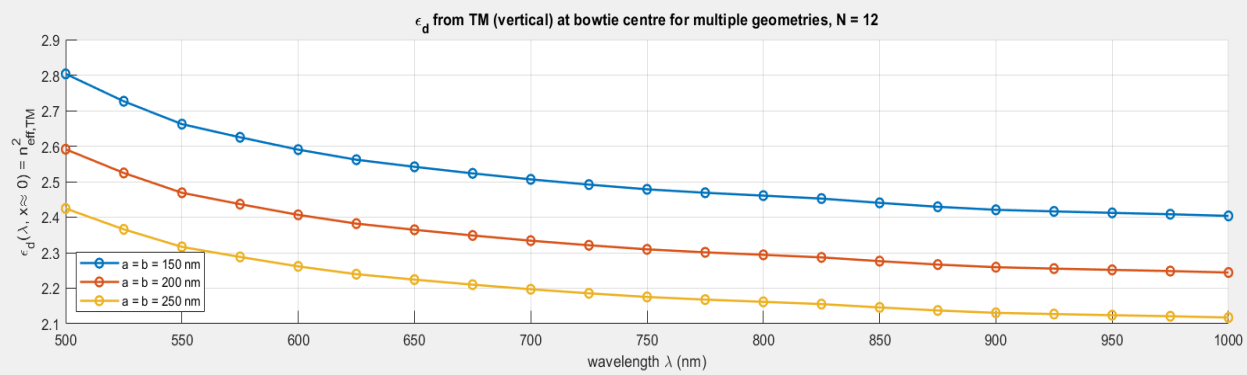

Fig. 7. Results for the TM Mode Implementation of the Modified Effective Index Method on the Bowtie Aperture

The TM Mode effective index monotonically decreased with wavelength and noticed higher confinement for smaller apertures. As the wavelength increased, field confinement in the slot weakened, and the mode approached a long-range SPP limit, reducing the effective index. Also, the $a = b = 150nm$ structure consistently showed the largest ϵ_d, with the value decreasing at $200\ nm$ and $250\ nm$, consistent with plasmonic slot-waveguide theory.

Before applying MEIM to the bowtie geometry, a rectangular aperture "sanity check" was performed. The same TM solver was run for a rectangular MIM slot. The dimensions were taken from Gordon and Brolo [4], which had four rectangular dimensions. The aperture width was kept constant at $270\ nm$ whereas the aperture height was varied in increments of $40\ nm$ in the range of $105\ nm$ to $225\ nm$.

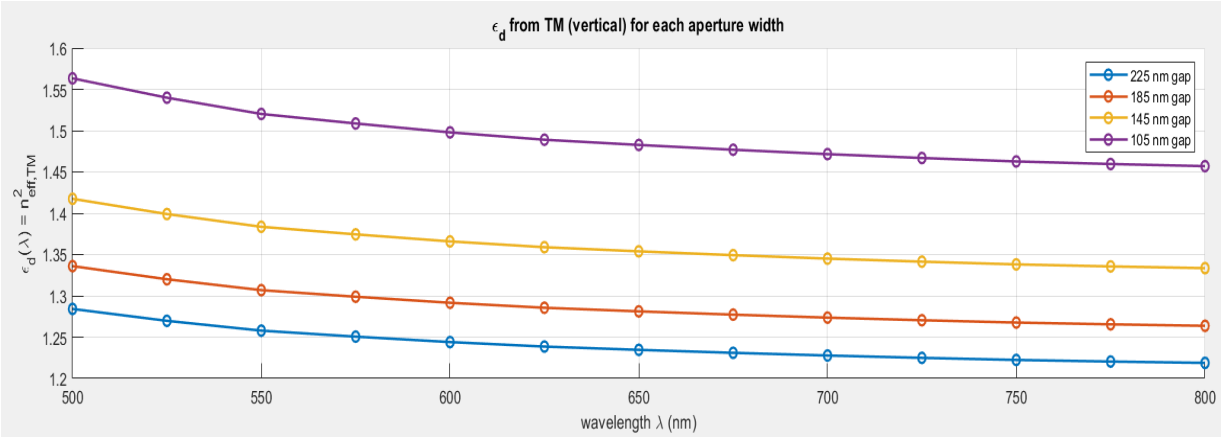

Fig. 8. Validation of TM Mode using a Rectangular Aperture

As shown in Fig. 8, the code reproduced the correct wavelength dependence and yielded values consistent with the literature for symmetric MIM slots. This confirmed that the TM tanh solver

was functioning correctly for multiple geometries. It also ensured that the permittivity data were properly interpreted.

4.3. Effective Index using TM-TE Mode and Validation

After establishing the TM-mode baseline, the TE contribution was introduced to account for hybridized electric-field components across the lateral direction of the aperture. The TE addition in the Modified Effective Index Method (MEIM) captures how the field spreads across the varying aperture width as the bowtie expands from its nanoscale apex. Using the TM-derived effective permittivities, the TE mode was computed through a multi-slab transfer-matrix method (TMM). Each lateral slice had permittivity $\epsilon_{d,i} = \eta^2_{eff,TM}(\lambda, x_i)$, and the metal on both sides was modelled using the same silver permittivity dataset.

A TE mode is only supported when the field that emerges into the left metal has no backward-decaying component, as mentioned in Eq. 20. This condition enforces guided-mode behaviour in a metal–dielectric–metal system. The TE Mode results exhibited two key trends, as seen in Fig. 9.

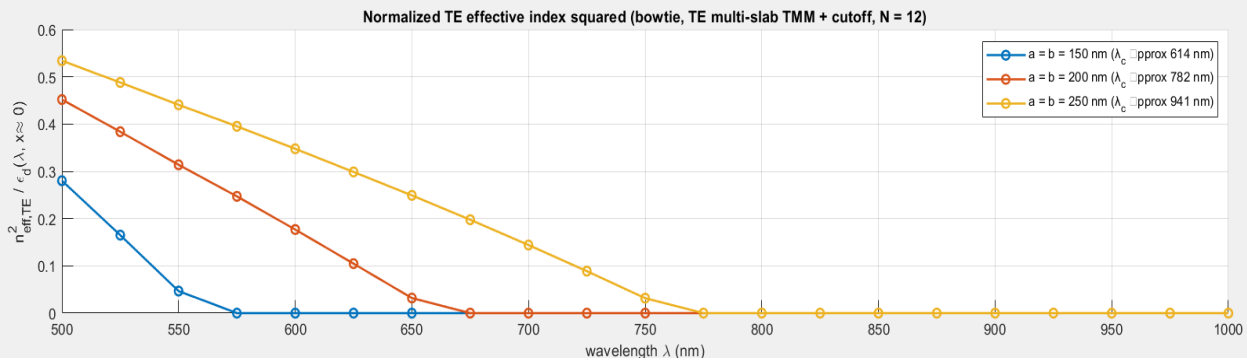

Fig. 9. Results for TM-TE Mode Implementation of the Modified Effective Index Method on the Bowtie Aperture

The TE Mode contributed to a rapid decline in η_{eff} with wavelength because longer wavelengths couple less efficiently into the laterally confined slab-like structure, reducing the TE effective index. Each geometry exhibited a wavelength beyond which no guided TE solution existed. The cutoff shifted to shorter wavelengths as the aperture decreased, as expected for dielectric slab waveguides.

A similar rectangular aperture “sanity check” was performed for the TE Mode, as shown in Fig. 10. The dimensions were the same as those used for the TM Mode validation.

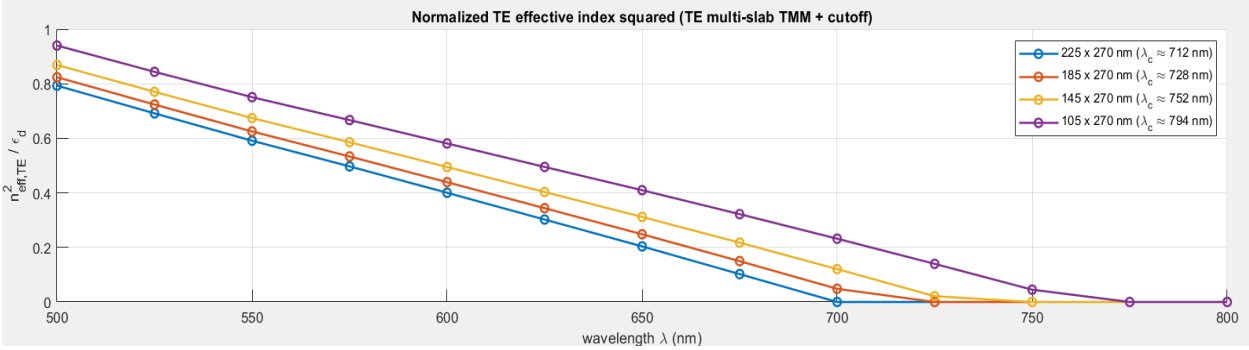

Fig. 10. Validation of TM-TE Mode using a Rectangular Aperture

The cut-off wavelength matched analytical expectations, and it was proven that the MEIM-TMM pipeline was correctly implemented.

4.4. Fabry-Pérot Resonance Comparison with Literature

To assess how well the MEIM–TMM model captures longitudinal resonances, the Fabry–Pérot (FP) condition was evaluated using:

$$k_z(\lambda)t = m\lambda, \quad k_z = \frac{2\pi}{\lambda}\eta_{eff}(\lambda) \tag{22}$$

for the fundamental mode $m = 1$ and a film thickness $t = 200$ nm.

Geometry Size	λ_{FP}
$a = b = 150nm$	$639\ nm$
$a = b = 200nm$	$618\ nm$
$a = b = 250nm$	$601\ nm$

Table. 01. Fabry-Pérot Wavelengths for various Bowtie Aperture Sizes

Ding et al. report that Fabry-Pérot (FP) peaks appear in reverse order, with the smallest aperture $(150\ nm)$ resonating at the lowest wavelength and the largest $(250\ nm)$ at the highest. This trend is due to the hybrid plasmonic surface modes and phase accumulation at metal boundaries, which shift the FP resonance upward as the cavity widens. In contrast, the MEIM calculation evaluates the TM mode only at the aperture center, excluding lateral plasmonic contributions from the bowtie sidewalls. While this model qualitatively reproduces the FP mechanism, it does not reproduce the exact ordering observed in full-wave simulations. However, the predicted FP wavelengths ($\approx 600 - 650\ nm$) align with experimental and FDTD results in the literature, confirming that the extracted effective refractive index η_{eff} values are valid.

5. DISCUSSIONS

The numerical investigation of bowtie aperture waveguides using the modified Effective Index Method (MEIM) revealed several important considerations regarding discretization strategy, TE-mode stability, the behaviour of the transfer-matrix residual near cut-off, and the limitations inherent in using 1D slab approximations to model inherently 2D plasmonic geometries. This section consolidates the observations from the modelling process and provides justifications for the numerical choices used in the final simulations.

5.1. Choice of Discretization and the Role of Slice Count

One of the most significant practical challenges encountered was selecting an appropriate number of discretized lateral slabs, N, for representing the bowtie taper using a staircase approximation. The initial implementation used 100 slices to maintain high resolution. However, it was observed that the TE-mode results developed pronounced spikes and oscillations when using large slice values.

5.1.1. Instability Condition during TM-TE Mode Simulation

Near cut-off, the TE mode became extremely sensitive to slight variations in the propagation constant β, causing the transfer-matrix element M_{21} to oscillate rapidly. When too many slabs were used, these oscillations became numerically stiff, and the optimizer (symbol “fminbnd” in the code) frequently locked onto shallow, non-physical local minima. This produced isolated spikes in the extracted $\eta_{eff,TE}$ curve, even though the underlying physics is smooth. The field is highly sensitive to small structural variations and to the oscillatory behaviour of the transfer matrices.

A surprising observation was that even numbers of slices (2, 4, 6, 8, 10, 12) yielded smooth TE curves, while odd values tended to introduce spikes. This behaviour can be traced back to symmetry. The bowtie aperture is symmetric about the vertical plane at $x = 0$. When an even number of slices is used, the staircase representation contains two central slabs symmetrically positioned around the centre, thus preserving the natural left–right symmetry of the physical structure. In contrast, an odd number of slices places a single slab at the centre, creating an asymmetric interface sequence that disrupts cancellation effects between adjacent interface and propagation matrices. To prevent oversimplification of the bowtie taper and eliminate the spikes in η_{eff}, 12 lateral slabs were used, as shown in Fig. 11.

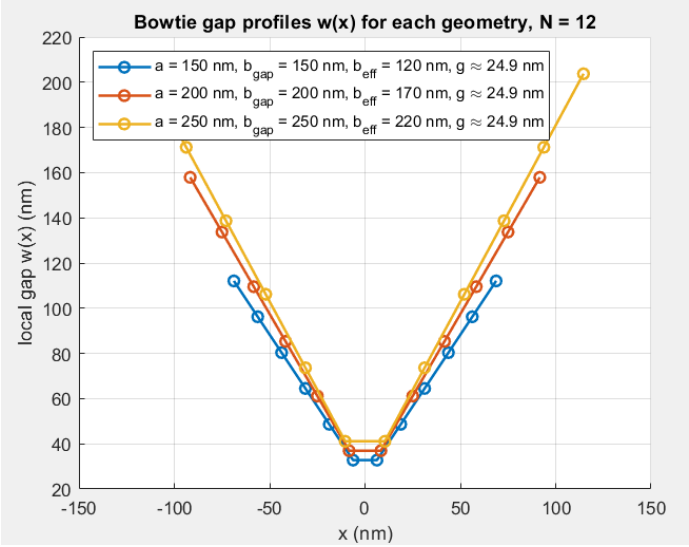

Fig. 11. Bowtie Gap Profiles for various sizes where $N = 12$.

5.1.2. Incorporating Metal Fillet Effects via Effective Height

In the bowtie geometry, the outer metal curvature defined by the fillet radius f is not explicitly included in the numerical model. Instead, its effect is incorporated indirectly by using an effective height $b_{eff} = b_{gap} - 30nm$ for each aperture size. This adjustment accounts for the fact that the rounded metallic boundaries reduce the portion of the aperture that behaves as a dielectric channel for TE propagation. While the geometric gap height b_{gap} corresponds to the complete metal-to-metal separation relevant for TM plasmonic confinement, the TE mode should only operate over the region where the field can penetrate before encountering the curved Ag surfaces. Using b_{eff}, therefore allows the TE multi-slab solver to remain physically meaningful without explicitly modelling the curvature, providing a consistent approximation across all bowtie sizes.

5.2. TM and TE Mode Behaviour and Numerical Stability

The TM field distributions across the vertical direction exhibit the expected plasmonic confinement at the metal–dielectric interfaces for all discretized slices, as shown in Fig. 12. The fields decay smoothly away from the interfaces and remain symmetric about the center of the aperture, consistent with the fundamental TM mode supported by a metal–dielectric–metal waveguide. This confirms that the vertical TM solution used to construct the effective dielectric profile $\epsilon_d(x)$ is physically robust and numerically stable.

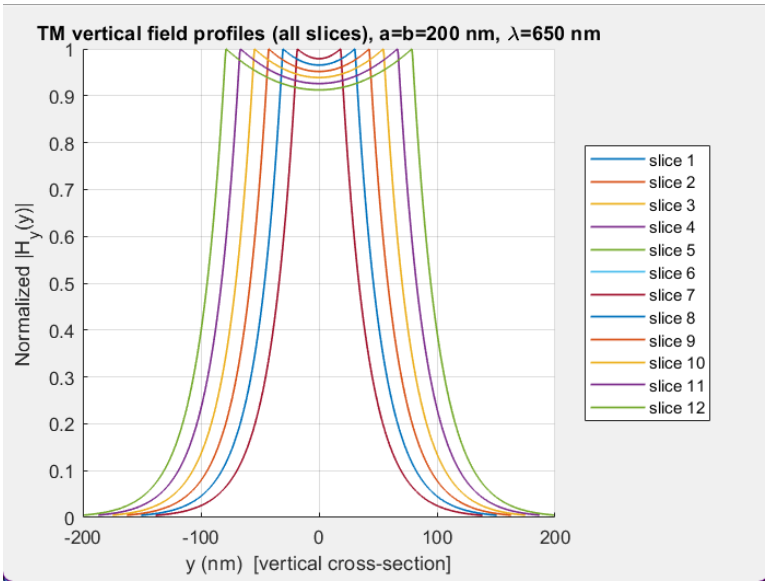

Fig. 12. TM Field profile across $N = 12$ slabs for $\lambda = 650nm$ and bowtie dimensions of 200 nm

In contrast, the TE field profiles in the lateral direction reveal more complex behavior. While the fundamental TE mode is symmetric and exhibits a maximum at the center of the aperture ($x = 0$), it was observed that, for certain wavelength ranges and increased discretization, the solver converges to an odd TE mode, as shown in Fig. 13. This mode is characterized by a clear node at the center of the aperture and antisymmetric field distribution about $x = 0$.

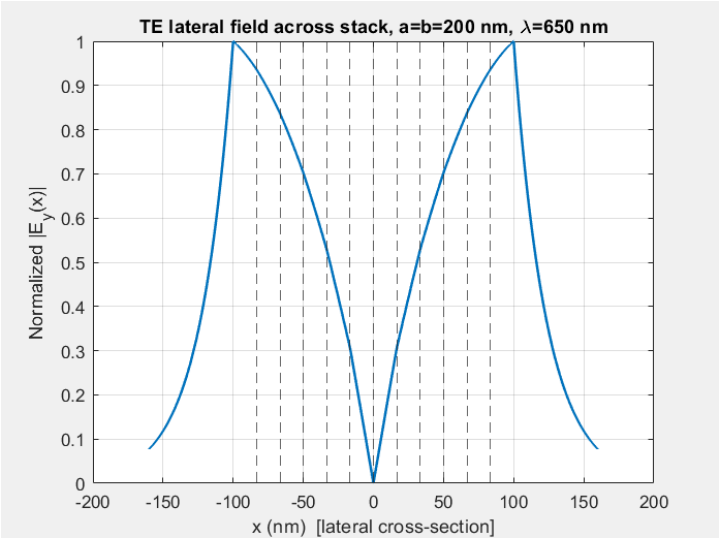

Fig. 13. TE Field profile across $N = 12$ slabs for $\lambda = 650nm$ and bowtie dimensions of 200 nm

The emergence of this odd TE mode indicates mode switching. As the geometry varies laterally in the bowtie aperture, the effective refractive index profile seen by the TE solver becomes weakly

guiding and highly sensitive to discretization. In this regime, multiple lateral TE eigenmodes can exist with closely spaced effective indices, making the solver susceptible to converging to a higher-order mode instead of the fundamental one.

Attempts to explicitly constrain the solver to track the fundamental TE mode resulted in increased oscillations in the effective index trends, suggesting that aggressive mode-tracking can introduce artificial discontinuities when the physical TE contribution is already approaching cutoff. Consequently, the observed spikes in the TE effective index are attributed to mode competition near cutoff, rather than to numerical instability or failure of the underlying TM–TE effective index framework.

6. CONCLUSION

This work developed and validated a Modified Effective Index Method (MEIM) framework for modelling nanoscale bowtie aperture waveguides using a combined TM–TE semi-analytical formulation. The bowtie geometry supports highly confined plasmonic modes whose behaviour cannot be captured by simple dielectric waveguide approximations. The modelling challenge arises from simultaneously handling strong material dispersion, abrupt geometric tapering, and sub-cutoff effects, all while retaining numerical stability. The approach presented in this project successfully addressed these challenges by integrating TM vertical confinement using a three-layer MIM dispersion model and TE lateral confinement using a multi-slab transfer-matrix method (TMM), both applied over a staircase discretization of the bowtie structure.

A significant outcome of this work is that the TM mode alone provides a stable and physically consistent estimate of the local effective permittivity ϵ_d across the wavelength range of 500–1000 nm. Because the bowtie gap varies gradually from its minimum value at the centre to its maximum at the edges, the TM mode captures a predictable monotonic decrease in ϵ_d with increasing wavelength, reflecting the weakening of plasmonic confinement as the frequency approaches the near-infrared regime. This behaviour aligns with classical plasmonic theory and the Johnson-Christy dispersion for silver. The TM formulation is also physically appropriate for this work because it directly corresponds to the vertical metal–insulator–metal (MIM) cavity, and because the tanh type dispersion relation remains stable for gaps above ~20–30 nm, the exact range used here.

The TE mode was introduced to account for lateral confinement along the aperture width, where the geometry cannot be approximated as a simple parallel-plate slab. The lateral taper of the bowtie was handled using a staircase approximation, and each slice was treated as a uniform slab with its own locally computed ϵ_d value. A global transfer matrix was constructed from these slices, and the TE effective index was obtained by enforcing the boundary condition that the backward-traveling wave must vanish in the metal on the opposite side. This non-linear residual minimization is sensitive to numerical stiffness, especially near the cutoff wavelength, where guided modes transition to radiation modes. The study showed that excessive lateral discretization, such as using 50–100 slices, amplifies this stiffness and produces unphysical spikes in $\eta_{eff,TE}$ due to the optimizer locking onto local minima of the residual. Reducing the discretization to an optimally

chosen 12 slices produced smooth, monotonic TE-mode curves that matched the expected physical trend and agreed with rectangular-slab validation tests. Because the rectangular aperture represents the ideal case of zero geometric taper, its smooth and spike-free TE curves confirmed that the underlying TE formulation was correct, and that the oscillations observed in early bowtie simulations were purely numerical artifacts caused by oversampling.

An important part of this study was validating the computed dispersion curves through comparison with Fabry–Pérot (FP) resonance wavelengths reported in the literature. Using the computed effective index values, resonance points corresponding to $k_z t = m\pi$ were extracted for film thickness $t = 200\,nm$. The analysis based on the extracted $\eta_{eff}(\lambda)$ values did not reproduce the resonance ordering reported by Ding et al., where larger bowtie apertures exhibit a clear red-shift. In our MEIM results, the FP wavelengths for the 150 nm, 200 nm, and 250 nm apertures do not follow this monotonic trend. This mismatch indicates that, although MEIM captures the general dispersion behaviour, small numerical variations in η_{eff} significantly affect the FP condition in these plasmonic cavities. As a result, the simplified MEIM framework is sufficient for modal dispersion analysis but not fully reliable for quantitatively predicting Fabry–Pérot resonance wavelengths in bowtie apertures.

In addition to reproducing the expected plasmonic dispersion, the model revealed several practical insights into bowtie aperture design. Larger apertures were found to support less confined but more slowly varying modes. In comparison, smaller apertures, particularly those near 150 nm, produce higher ϵ_d and stronger confinement but also shorter effective propagation lengths due to increased modal absorption in silver. The TE analysis further showed that even moderate geometric tapering, as seen in bowtie structures, introduces strong lateral sensitivity, making the modal behaviour more susceptible to numerical cutoff effects than in rectangular apertures. By choosing an appropriate discretization, these effects were controlled without sacrificing geometric fidelity.

Overall, this work demonstrates that an appropriately constructed TM–TE Modified Effective Index Method can reliably model plasmonic bowtie apertures across a broad wavelength range without requiring full FDTD or FEM simulations. The method is computationally lightweight, physically interpretable, and adaptable to related nanoplasmonic structures such as double nanoholes, slot waveguides, or tapered trenches. Future extensions of this work may include incorporating the imaginary part of ϵ_d directly into the TE solver for loss-aware propagation,

exploring nonlocal or quantum-corrected metal permittivity models, or validating the MEIM predictions against full-wave solvers such as Lumerical MODE Solutions.

By carefully balancing analytical tractability with geometric realism, this MEIM framework provides a valuable and scalable tool for understanding modal behaviour in nanoscale plasmonic apertures. It offers an efficient pathway for preliminary design, optimization, and physical interpretation of complex metallic nanostructures central to sensing, focusing, and light-concentrating applications.

REFERENCES

[1] Singh, S., "Refractive Index Measurement and its Applications," Physica Scripta, 65(2), 167–180 (2002).

[2] Chiang, K. S., "Effective-Index Method for the Analysis of Optical Waveguide Couplers and Arrays: An Asymptotic Theory," Journal of Lightwave Technology, 9(1), 62–72 (1991).

[3] Pogossian, S. P., Gall, H. L., Gieraltowski, J. and Loaëc, J., "Determination of the parameters of rectangular dielectric waveguides by new effective index methods," Journal of Modern Optics, 42(2), 403–409 (1995).

[4] Gordon, R. and Brolo, A., "Increased cut-off wavelength for a subwavelength hole in a real metal," Optics express, 13(6), 1933–1938 (2005).

[5] Lifante, G., "Effective Index Method for Modelling Sub-Wavelength Two-Dimensional Periodic Structures," Physica Scripta, T118, 72–77 (2005).

[6] Moskalev, D., Kozlov, A., Salgaeva, U., Krishtop, V. and Volyntsev, A., "Applicability of the Effective Index Method for the Simulation of X-Cut $LiNbO_3$ Waveguides," Applied Sciences, 13(11), 6374, 1–13 (2023).

[7] Zhang, E., Zhu, X. and Zhang, L., "Effective and group refractive index extraction and cross-sectional dimension estimation for silicon-on-insulator rib waveguides." Optics Express, 32(18), 31375, 1–14 (2024).

[8] Snyder, A. W., "Coupled-Mode Theory for Optical Fibers," Journal of the Optical Society of America, 62(11), 1267–1277 (1972).

[9] Butler, J. K., Ackley, D. E. and Botez, D., "Coupled-mode analysis of phase-locked injection laser arrays," Applied Physics Letters, 44(3), 293–295 (1984).

[10] Ding, L., Qin, J., Guo, S. et al, "Resonant Effects in Nanoscale Bowtie Apertures," Sci Rep, 6, 27254 (2016).

[11] Genet, C. and Ebbesen, T. W., "Light in tiny holes," Nature, 445, 39–46 (2007).

[12] Degiron, A. and Smith, D. R., "Numerical simulations of long-range plasmons," Optics Express, 14, 1611–1625 (2006).

[13] Biagioni, P., Huang, J. S. and Hecht, B., "Nanoantennas for visible and infrared radiation," Rep. Prog. Phys. Soc. 75, 024402 (2012).

[14] Ding, L. and Wang, L., "Numerical and experimental study of nanolithography using nanoscale C-shaped aperture," Applied Physics. A. 119, 1133 (2015).

[15] Marcatili, E. A. J., "Dielectric rectangular waveguide and directional coupler for integrated optics," Bell System Technical Journal, 48(7), 2071–2102 (1969).

[16] Snyder, A. W. and Love, J. D., "Optical Waveguide Theory," Springer (1983).

[17] Sheppard, C. J. R. and Saghafi, S., “Transverse-electric and transverse-magnetic beam modes beyond the paraxial approximation,” Optics Letters, 24(22), 1543 (1999).

[18] Angulo Barrios, C., “An Analysis of a Compact Label-Free Guiding-Wave Biosensor Based on a Semiconductor-Clad Dielectric Strip Waveguide,” Sensors, 20(12), 3368 (2020).

[19] Buus, J., “The Effective Index Method and Its Application to Semiconductor Lasers,” IEEE Journal of Quantum Electronics, 18(7), 1083–1089 (1982).

[20] Chiang, K. S., “Analysis of rectangular dielectric waveguides: The effective index method with improved accuracy,” IEEE J. Lightwave Technol., 3(2), 385–390 (1985).

[21] Ramaswamy, R. V and Srivastava, R., “Analysis of rib waveguides by effective index method,” Opt. Quantum Electron., 11, 407–414 (1979).

[22] Marcuse, D., “Theory of Dielectric Optical Waveguides,” Academic Press, 2 (1991).

[23] Belhadj, W., “On the Validity of the Effective Index Method for Long Period Grating Photonic Crystal Fibers,” Materials Sciences and Applications, 3(5), 310–316 (2012).

[24] Kumar, A. and Srivastava, R., “Iterative effective index method for optical rib waveguides,” IEEE J. Lightwave Technol., 21(3), 726–732, (2003).

[25] Oulton, R. F. et al., “A hybrid plasmonic waveguide for subwavelength confinement and long-range propagation,” Nature Photonics, 2(8), 496–500 (2008).

[26] Berini, P., “Figures of merit for surface plasmon waveguides,” Optics Express, 14(26), 13030–13042 (2006).

[27] Johnson, P. B and Christy, R. W., “Optical Constants of the Nobel Metals,” Phys. Rev. B, 12, 4370–4379 (1972).

[28] Raghunandan, K., “Introduction to Wireless Communications and Networks,” Springer (2022).